

Alignment Mirror Mechanisms for Space Use

Bruno M. Jau, Colin M. McKinney, Robert F. Smythe, Dean Palmer
Jet Propulsion Laboratory
California Institute of Technology
4800 Oak Grove Drive
Pasadena, CA 91109
(818) 354-1875
bjau@jpl.nasa.gov

Abstract—The paper describes an optical Alignment Mirror Mechanism (AMM), and discusses its control scheme. The mirror's angular positioning accuracy requirement is ± 0.2 arc-sec. This requires the mirror's linear positioning actuators to have a positioning accuracy of ± 109 nm to enable the mirror to meet the angular tip/tilt accuracy requirement. Demonstrated capabilities are ± 35 nm linear positioning capability at the actuator, which translates into ± 0.07 arc-sec angular mirror positioning accuracy.

The mechanism consists of a structure with sets of cross directional flexures that enable the mirror's tip and tilt motion, a mirror with its kinematic mount, and two linear actuators. An actuator is comprised of a brushless DC motor, a linear ball screw, and a piezoelectric brake that holds the mirror's position while the unit is unpowered. An interferometric linear position sensor senses the actuator's position.

A closed loop, custom electronics design was implemented that drives four motors, or two AMMs. The electronics are comprised of four redundant brushless DC motor drive channels, optical quadrature encoder feedback, piezoelectric brake drive circuitry, and a Field Programmable Gate Array (FPGA) to provide digital control, communication, and housekeeping for the board. The closed loop functionality of a motor channel is accomplished within the FPGA by custom controller firmware, developed at JPL.^{1,2}

TABLE OF CONTENTS

1. INTRODUCTION	1
2. THE ASTROMETRIC BEAM COMBINER (ABC) BENCH ...	1
3. KEY REQUIREMENTS	4
4. MECHANICAL DESCRIPTION	4
5. ELECTRONIC CONTROLLER	7
6. TEST RESULTS	9
7. LESSONS LEARNED	11
8. SUMMARY	12
REFERENCES	12
BIOGRAPHY	12
ACKNOWLEDGEMENTS	13

1. INTRODUCTION

Alignment mirrors have the task to maintain precise

alignment of a light beam to an optical target over time. The mechanical challenge in creating such devices is to develop a mechanism that has mirror-positioning resolutions to the required accuracy; whereas the control electronics challenge is to develop a real time, closed loop control electronics system that can evaluate the position sensor, and position the mirror to the required accuracy at the required speed.

The AMMs being described in this paper were developed for an Astrometric Beam Combiner (ABC) optical bench, which is part of an interferometer development. Custom electronics were also developed to accommodate the presence of multiple AMMs within the ABC and provide a compact, all-in-one solution to power and control the AMMs. The paper will describe both, the mechanical device, and its control.

2. THE ASTROMETRIC BEAM COMBINER (ABC) BENCH

In an interferometer, starlight is reflected by two telescopes (Siderostats), it then passes by (or through) a variety of optical devices, like relay optics, and beam compressors, before it enters the ABC bench.

The ABC bench is the heart of the interferometer. It combines the two light beams, enabling combined, or interference fringe measurements at the focal plane. The ABC's main components are beam combiners, fringe trackers (the optical sensors, or detector arrays, or cameras of the interferometer), alignment optics, and a metrology system.

Four custom designed, identical AMMs are incorporated in this flight-like ABC bench that was developed at JPL, to demonstrate that interferometric technology is feasible and mature for space implementation. Fig. 1 shows a schematic diagram of the ABC bench, indicating the locations of the four AMMs, Fig. 2 is a CAD model of the bench, and Fig. 3 is an actual picture of the ABC bench, taken during vibration testing. A detailed description of the entire interferometer can be found in Ref. [1].

¹978-1-4244-7351-9/11/\$26.00 ©2011 IEEE.

² IEEEAC paper #1268, Version 2, Updated Dec 13, 2010

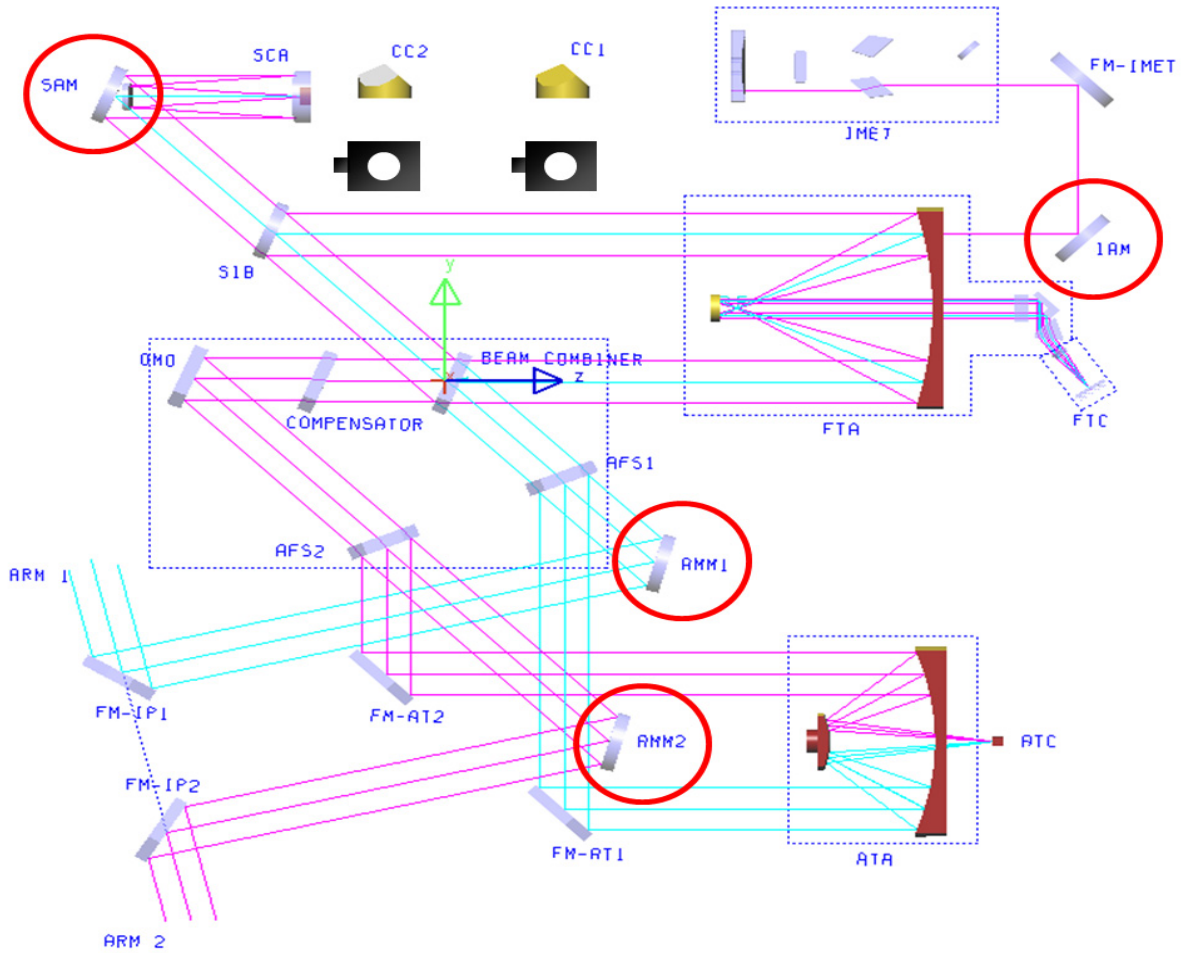


Fig. 1: Beam Path Schematic of the Astrometric Beam Combiner Bench

Acronyms of the ABC Components:

The four Alignment Mirrors:

AMM 1, 2 Alignment Mirror Mechanisms
 IAM Int. Metrology AMM
 SAM Stimulus AMM

Other ABC Components:

ATA Angle Tracker Assembly
 ATC Angle Tracking Camera
 CC 1, 2 Corner Cubes
 CCA Compensated Combiner Assembly
 FM-AT 1, 2 Fold Mirror for Angle Tracker
 FM-IMET Fold Mirror for iMET
 FM-IP 1, 2 Fold Mirrors for Inlet Port
 FTA Fringe Tracker Assembly
 FTC Fringe Tracking Camera
 iMET Internal Metrology Beam Launcher
 SCA Stimulus Collimator Assembly
 SIB Stimulus Injection Beam Splitter



Fig. 2: The Components in the ABC Optical Bench

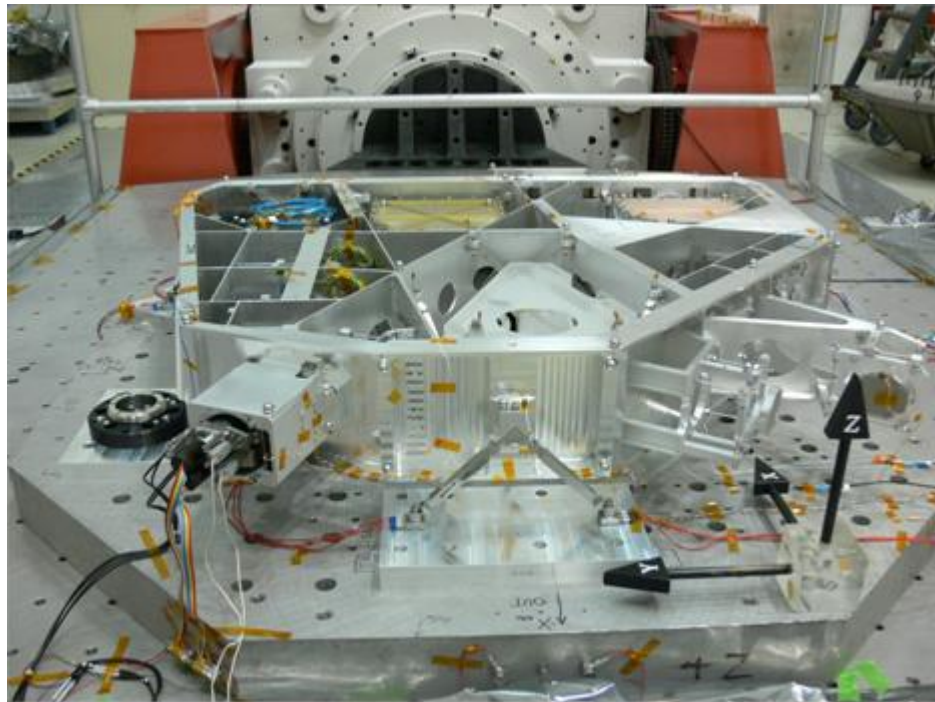


Fig. 3: The ABC Bench on the Shaker Table, ready for Vibration Testing
(One of the AMMs is at front left)

3. KEY REQUIREMENTS

The principal requirements for the AMMs are:

- Beam Foot Print on the Mirror: 53.5 mm
- Tip/Tilt Range of Motion: ± 2 mrad (± 412 arc-sec)
- Tip/Tilt Positioning Accuracy, Repeatability and Resolution: $< \pm 1$ μ rad (± 0.206 arc-sec)
- Mirror piston positioning accuracy $\pm .025$ mm
- Operational Temperature Range 15-25 degC

4. MECHANICAL DESCRIPTION

The Mechanical Assembly

The AMM is a two degree of freedom gimbal device, capable of positioning the mirror to within a fraction of an arc-sec. It is depicted in Figs 4 and 5; while Fig. 6 shows a cross sectional view through the mechanism. A cleverly designed titanium part, partitioned into four sections, is the structural backbone of the assembly. Its complex shape was formed through electro discharge machining (EDM). It consists of: 1) Four structural mounts, which are connected to the main platform through flexures. 2) The main platform, to which the lower actuator is attached. 3) The lower pivot table, linked to the main platform through two flexures that enable the lower table to pivot around one axis in accordance with the lower actuator's movements. The upper pivot actuator is also attached to the lower pivot table; it provides the pivoting capability for the upper table. 4) The upper pivot table, linked to the lower table through another two flexures, clocked 90 degrees apart from the lower flexures, thus enabling the upper table to pivot in the cross directional axis.

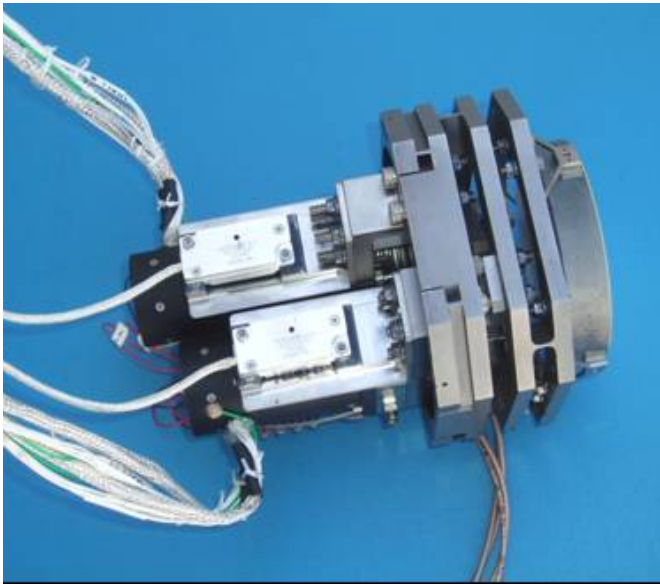


Fig. 4: The AMM, viewing the Position Sensor side

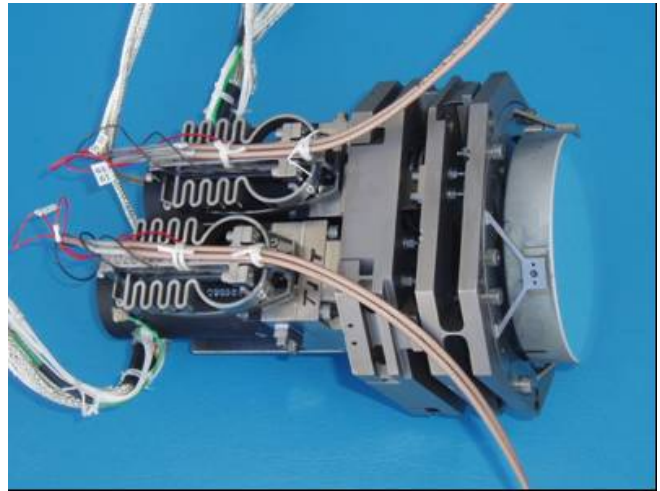


Fig. 5: The AMM, viewing the Brake side

The total mass of the AMM assembly is less than 1 kg. Its overall length is 130 mm.

The mirror is 63.5 mm in diameter and 12.7 mm thick, it is made of fused silica. It is linked to the structure by three sets of bipods. A custom designed fixture was used to position the mirror prior to bonding, ensuring its positional accuracy to be within the 0.025 mm tolerance w.r.t. the nominal height of the assembled stage.

Due to the criticality of maintaining the alignment through vibration testing, the connecting structural parts also feature bonding pockets to maintain positional stability, besides using fasteners in the traditional way. This proved very successful: the overall alignment and positioning over several components in the ABC bench shifted less than one pixel in the camera during vibration, which is less than 7.5 arc-sec of angular shifts over all components combined. This was much better than expected; it could easily be accommodated by this stage that has a range of motion of 300 arc-sec.

The actuator's output is coupled to the input pivot flexure, which is linked to a lever arm, called floating link. This flexure also enables the ball nut's linear motion to be transformed into a rotational motion at the lever arm. The lever arm's function is to reduce the motion amplitude by a factor of three, thus enhancing the angular positional resolution of the mirror by the same factor. It is suspended by a flexure as well. Another flexure, the upper of the two lever pivots in Fig. 6, serves as linkage between the lever arm and the corresponding mirror stage. The lever arms and their flexures are integral parts of the main structure, all shaped by EDM from the same structure.

Fig. 7 shows the structural parts of the AMM from the mirror side, with the mirror assembly removed. The lever arms are visible near the top of the structure.

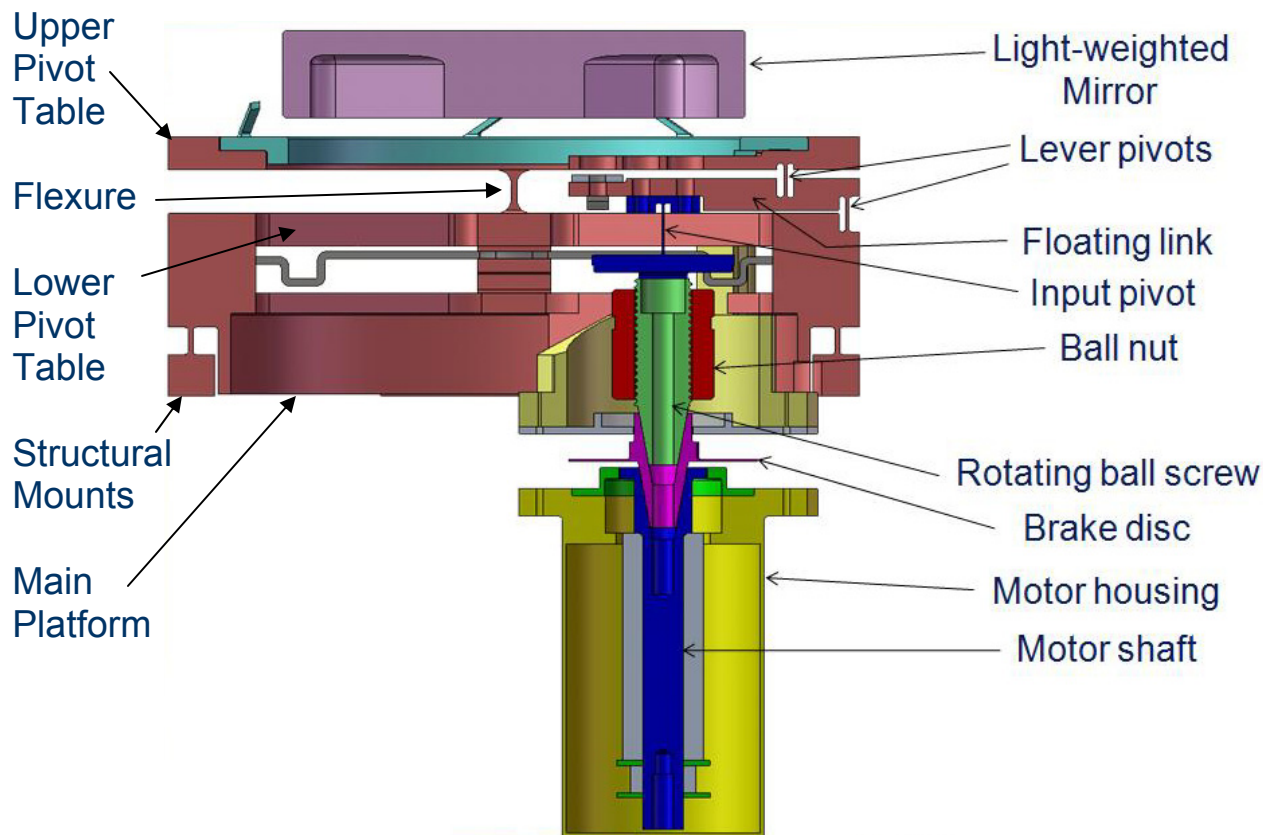


Fig. 6: Cross Section through Actuator and Parts of the Structure

The Actuator

Two four pole, three phase, brushless DC motors are used to position the mirror. The maximum resistance torque was computed to be 7 mN-m, the motor is rated at 21 mN-m, ensuring a larger than required 100% torque margin. The motor features redundant coils and redundant Hall Effect sensors. The motor output rotates the brake disk. The brake disk also has limit stops, restricting motor motions to less than a full turn. The brake disk drives the spindle (8 mm diameter lead screw with 1 mm pitch), moving the ball nut axially. The lube for the ball screw assembly is Braycote 601. A bellows, bonded to the brake housing and to the structure above the ball nut, prevents the ball nut from rotating, but allows axial displacements. Even though the ball nut was manufactured with a slight preload to operate backlash free, the bellows is assembled in a slightly compressed state to preload the ball nut to index in one axial direction only, thus further ensuring complete backlash free operations. An arm, mounted at the ball nut and extending backwards, serves as mounting platform for the sensor glass scale (see Position Sensor description). The sensor assembly shares the same mounting platform as the motor. The front of the actuator, including its bellows, can be seen in Fig. 7, from which the mirror assembly was removed. The actuators are shown in Fig. 8.



Fig. 7: The AMM with the Mirror Assembly removed

The relationship between the angular displacements at the mirror and the linear actuator motions are as follows:

- The full range tip or tilt angular mirror motion of ± 2 mrad requires ± 0.225 mm of ball nut travel, which corresponds to ± 81 deg of rotor rotation.

- The tip or tilt mirror positioning resolution of $\pm 1 \mu\text{m}$ corresponds to $\pm 0.1125 \mu\text{m}$ of nut travel, it requires ± 0.04 deg of rotor rotation.

With the demonstrated linear positional accuracy of ± 50 nm, the rotor can be electronically controlled to ± 0.017 deg! This is quite remarkable.



Fig. 8: The Actuators

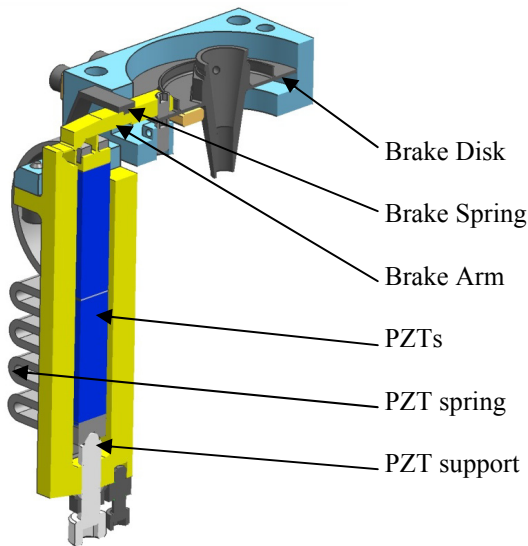


Fig. 9: Cross Section through the Brake

The Brake

A disk-type brake, having one actuated brake shoe, is used. A passive brake shoe at the other side of the brake disk, opposite the active brake shoe, prevents the thin walled brake disk from deflecting beyond the nominal gap between disk and passive brake shoe, with the gap being less than 20 μm . A preload spring provides the clamping force for the brake. This force remains applied when the brake is unpowered. Two Piezo-Electric (PZT) actuators in series

actuate the brake. Each receives an input of 100 V to deploy to its full stroke of 12 μm . With the lever arm extending to the brake shoe, this translates to approx. 0.05 mm of axial travel per PZT at the active brake shoe. The PZT pushes off the ball joint interface below the PZT when actuated. The complex shaped spring keeps the PZTs in compression at all times (PZTs cannot be in tension). This complex shape was arrived at because of the spring constant and spring stiffness requirements. The brake holding torque is set to 15 N-mm, which is enough to prevent the spindle from being back-driven due to the applied preload, but it does not exceed the motor's torque capability, which could position the mirror even if the brake would fail in the applied position. Due to the soft pivoting flexures of the lever arm, other structural deflections, and the wobbling of the brake disk, it takes the stroke capability of both actuators to release the brake, which was not planned. One PZT was meant to be a redundant back-up. A cross section through the brake can be seen in Fig 9, the brake is also visible in Fig. 10.



Fig. 10: The Actuator with the Brake Exposed

The Position Sensors

Vacuum compatible, but otherwise standard production high-resolution optical encoders measure the linear motion of each actuator. The encoders are grating-based, reflective, interferometric encoders [2], consisting of three major components: the read head, a moving glass scale, and the remote control electronics. Light emitted from a source within the read head is incident on the scale. The scale, mounted to an arm that is moving with the ball nut, is a glass substrate containing a periodic grating structure. The incident light reflects and diffracts from the grating. The diffracted beam re-enters the sensor head and forms interference fringes on a detector array. The processing electronics calculate the interference fringe pattern's spatial

phase from the detector array signal. Scale movement results in fringe pattern movements across the detector array. The processing electronics re-analyze the resulting fringe pattern and produce a system output corresponding to the surface's new position.

The sensor measures the positioning of the spindle nut. The resolution to which this sensor can detect positional shifts is 1.2 nm. A homing mark in the glass scale is used to determine the absolute position of the actuator. Using this indexing feature, the accuracy to which the absolute position of the ball nut can be measured over short distances is 18 nm. The RMS of the mechanical positioning repeatability is 35 nm, or 0.7 arc-sec.

Thermal Effects

Due to the small environmental temperature range (the ABC bench-interior is kept to ± 1 degC); thermal distortions are not a problem for this small device. However, motor heating could influence mirror positioning. This is mitigated by using the structure as heat sink, conducting heat into the surrounding structure. It is further controlled by the low duty cycle of the motor, having an on time of less than 5%. Thermal effects were not noticed during integrated testing when the reflected optical beam was sensed.

Mechanical Testing/Qualification

Even though these devices are pre-flight, they went through similar testing/qualification as flight hardware would undergo. Functional testing consisted primarily of the positional accuracy determination, with results already provided in the sensor section above, and the electronics verification described below. The AMM mechanical hardware was vibration tested to the levels indicated in Table 1 below.

Axis	Frequency (Hz)		Random Level
all		20	+3 db/octave
	50	300	0.08
		2000	- 6 db/octave
	Overall Level		6.49 g_{rms}

Table 1: Vibration Testing Levels

5. ELECTRONIC CONTROLLER

Electronic Hardware

The application for the AMM required the custom design of

electronic hardware that would act as a stand-alone motor controller, taking in +28V spacecraft voltage and operating up to 2 AMMs, among other motor drive necessities. The motor controller board (hereby referred to as the Motorboard) contains the necessary hardware to drive the motors within the AMM and provide support for the Linear Quadrature encoders that enable the position feedback for the AMM. The Motorboard also provides the PZT brake circuitry, encoder inputs and control algorithms for complete closed-loop operation of one or more AMMs. At the heart of the Motorboard lies a Xilinx Virtex 4 FPGA that houses the essential motor control and housekeeping algorithms. Mention the fact that the Motorboard was designed to support a number of configurations (including limit switch) but the AMM did not support this feature.

Figure 11 shows the Motorboard electronics that are comprised of a standard 6U-size (6.3" x 9.1") double-sided PCB housing the motor drive electronics, voltage regulators, FPGA, housekeeping circuitry, and digital I/O. The front panel of the Motorboard (bottom of picture) houses the connectors for all eight Motors cables, four encoder cables, the RS-232 Serial port cable, and the optional Mis-Std 1553 connection. The rear panel (top of picture) houses the Power connector and two pairs of differential external sync inputs or outputs.

Control Algorithm within FPGA Firmware

A custom Proportional, Integral, Derivative (PID) controller housed within the FPGA firmware controls the AMM's tip and tilt stages. The PID varies voltage commands to each of the 3 motor windings of the Brushless DC (BLDC) 3-phase motors using either a trapezoidal commutation scheme or a sinusoidal commutation scheme. Trapezoidal commutation applies voltage based on each motor's Hall Effect sensors' timing signals. This yields a coarse voltage command of 24 steps per motor revolution. Alternatively, sinusoidal commutation uses the linear glass scale encoder output transposed to rotational increments to yield a fine voltage command of over 400,000 steps per revolution. The DC brushless motor back EMF (Electro-Magnetic Flux) is a sinusoidally varying voltage. Thus, by applying voltages to the windings in a sinusoidal manner the motor converts all of the applied current into output torque (ideally), rather than imparting unwanted radial forces to the drive shaft. Since all of the available current is being converted to torque, the torque variation, or torque ripple, is minimized. The elimination of torque ripple on the application is vital to achieve the AMM's exceptionally small pointing and jitter requirements.



Fig. 11: Top View of Motorboard

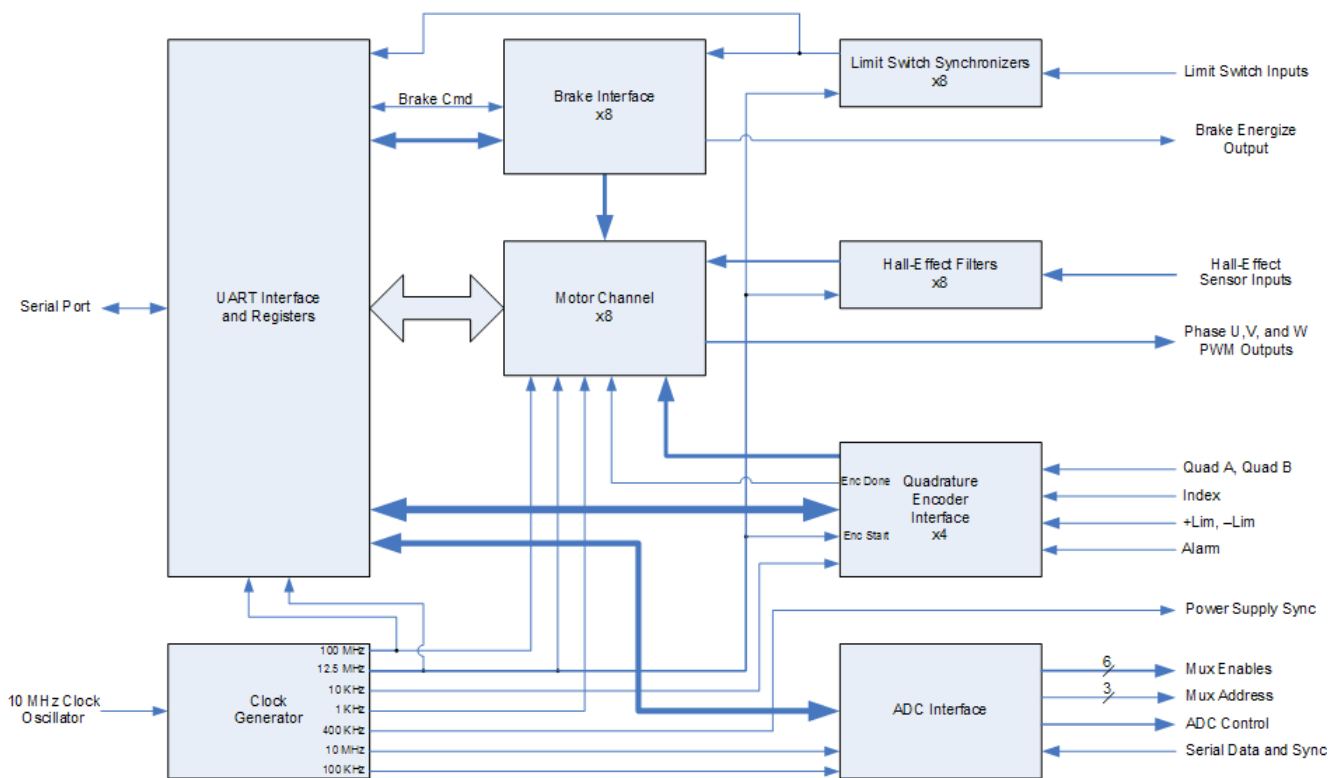


Fig. 12: FPGA Firmware Block Diagram

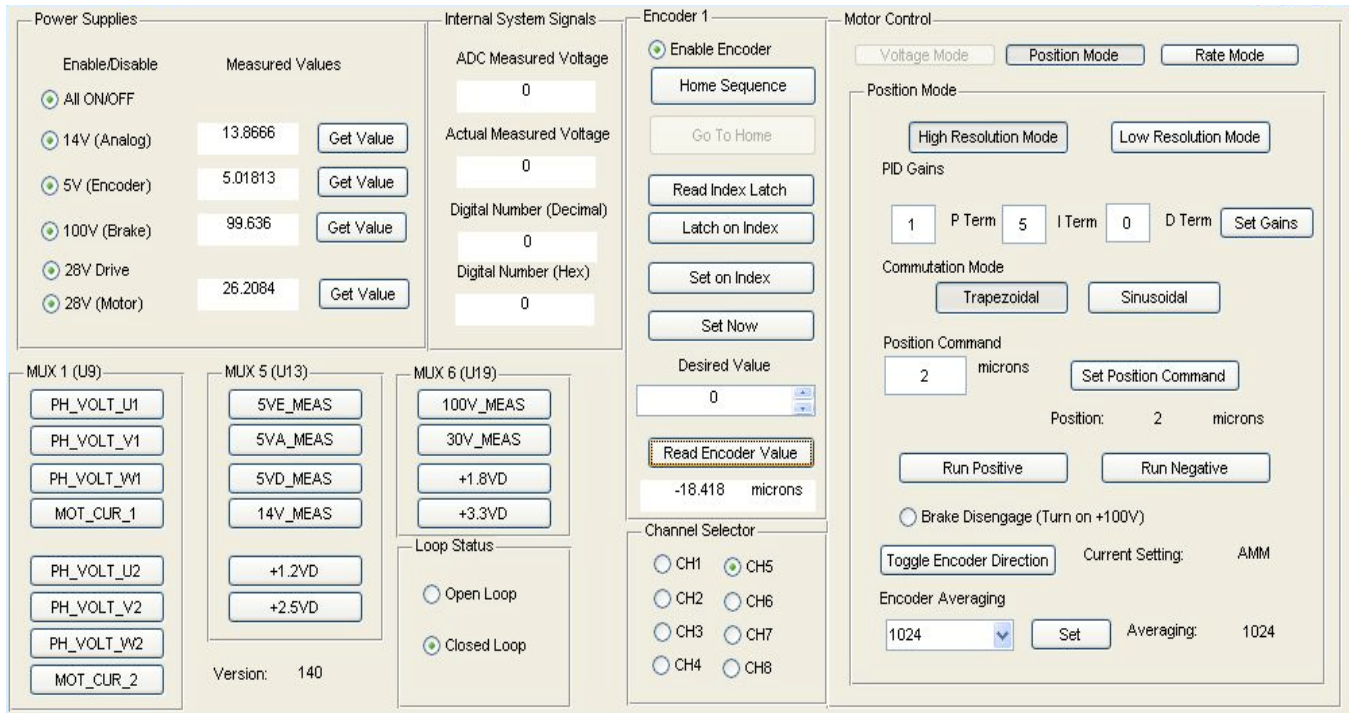


Fig. 13: Screen Capture of the Motorboard Graphical User Interface

FPGA Firmware Architecture

The FPGA houses many custom modules designed to interface to the peripherals within the Motorboard. A block diagram of the FPGA firmware architecture can be seen in Figure 12.

In order to support up to eight motors (or four redundant motor drive channels capable of driving two AMMs), the necessary firmware modules to interface to a single motor are duplicated eight times. These include PID control algorithm, brake interface, Hall sensor feedback, end of travel limit switch interface, and a single quadrature encoder feedback that covers two motors. While there is additional hardware on the Motorboard that supports a Mil-Std 1553 Interface and two Bi-Directional External Sync ports, this firmware was not necessary for AMM support and therefore was not included in this design.

Firmware to ensure the stability and operational control of the Motorboard is also included within the FPGA and will be referred to as the ‘housekeeping’ module. The housekeeping module monitors system voltages and currents and takes action to correct any out-of-bounds conditions found on the board. This is performed by way of Multiple Analog Multiplexors (MUXs) that interface to an Analog to Digital Converter (ADC). The ADC feeds the FPGA digitized system parameters for constant monitoring and fault protection.

Software for Manual Operation of the Motorboard

Finally, firmware for a Universal Asynchronous Receiver/Transmitter (UART) is provided to allow for manual use within a laboratory. The UART within the FPGA sends and receives external commands to a remote PC using a standard RS-232 serial port. This interface to the outside world provides the user the ability to debug and test the board using a custom Graphical User Interface (GUI) as seen in Figure 13.

The Motorboard GUI provides the user with the ability to check the status of the Motorboard Housekeeping signals, command the motors to perform open- or closed-loop discrete moves, and reports the feedback of the commanded moves for observation. This GUI was instrumental in the testing and verification of the AMM performance.

6. TEST RESULTS

AMM performance was tested and verified using the Motorboard electronics and the custom interface software. One complete AMM, comprised of two 3-phase BLDC motors, their respective quadrature encoders and brakes, were commanded and driven by the Motorboard. All positional results were gathered by two separate means of measurement – the encoder feedback as recorded by the Motorboard FPGA, in addition to a physical optical measurement using a precision autocollimator.

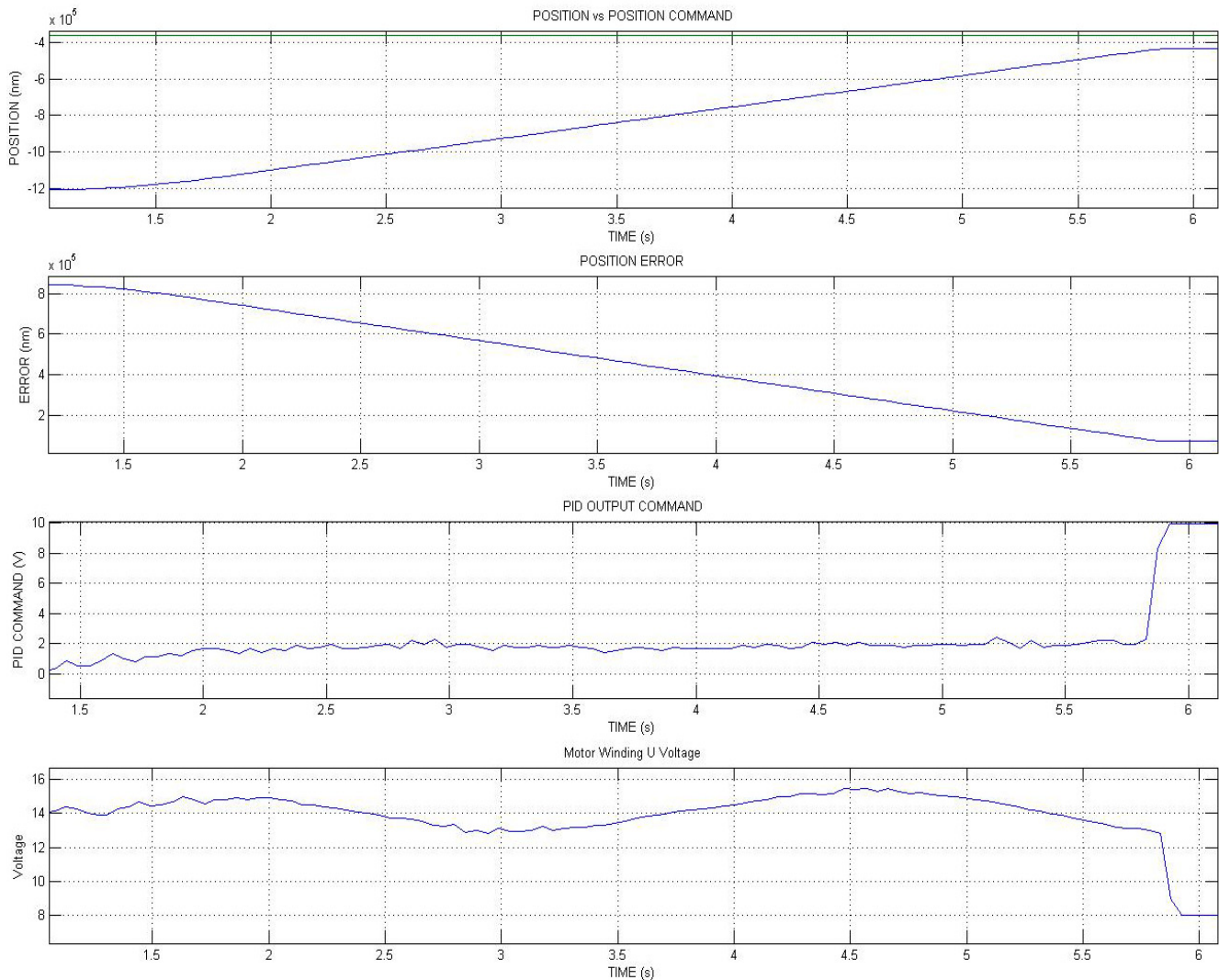


Fig. 14: Results of end-to-end Travel of AMM Stage using Sinusoidal Commutation

Verification of Design Features

Initial testing of the AMM was comprised of verifying core functionalities associated with its design, both mechanical and electrical. Parameters such as full range of motion, positioning resolution and accuracy, speed of travel, brake operation and the error induced were all factors in the successful characterization of the AMM and its performance.

Each of the two AMM stages has a full linear motion of approximately 800 μm end-to-end travel. Figure 14 depicts this range, showing the motor position travelling from one end of travel at -1200 μm to -400 μm at the opposite end of travel in the top of the four plots. The bottom-most plot of the four shows the Voltage output on one of the three motor phase windings across its range, the smoothness of the trace indicating that the motor is operating in Sinusoidal Commutation.

Steady-State Position Accuracy and Limitations

Each AMM motor stage was found to have a positional accuracy, on average, of +/- 25 nm. This number exceeded the requirements of positional accuracy for the testbed.

Overall positioning accuracy and steady state error was a function of PID controller resolution and mechanical displacement of the motor due to engagement of the brake. As seen in Figure 15, an AMM stage is driven to a commanded position and arrives to within ± 25 nm accuracy while being actively driven by the electronics. The metric in Plot 1 of this figure, 'Position vs. Position Command', relates to a solid green horizontal line that indicates where the target position is. The actual position is then plotted against that solid green line. When the actual position reaches the commanded position marker, the Error term in the second plot of Figure 15 goes to zero.

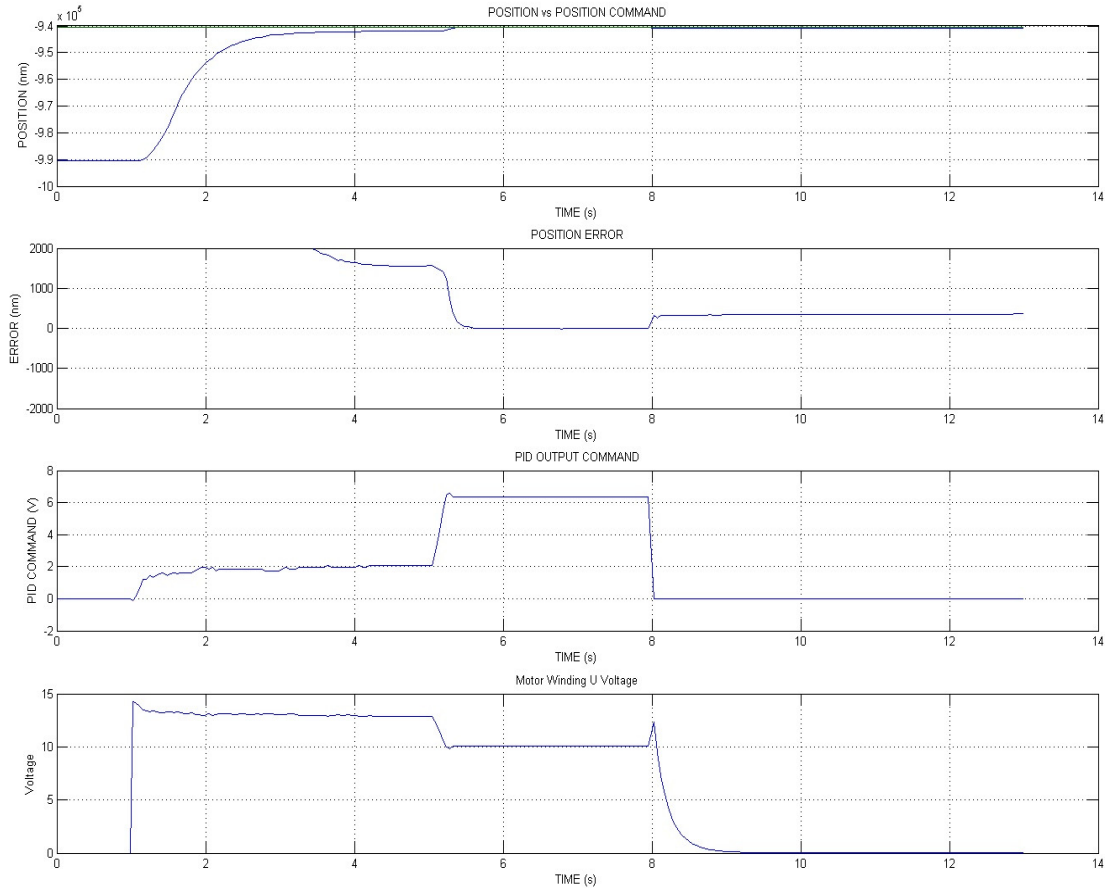


Fig. 15: Example of steady-state Error Displacement due to wind-up

One can see that just after the 5 second mark, the actual position of the motor has reached the commanded position and the error term is zero. However, once the brake is engaged and power is removed from the motor coils, a non-negligible linear displacement can be seen at 8 seconds in the second of four plots. This is believed to be attributed to the wind-up that occurs as the PID controller is fighting the engagement of the brake. When the brake is engaged, the PID controller must provide extra drive current to the motor windings to fight the increased load resistance and bring the motor to its final position with minimal error. The figure shows the motor reach its final position with almost 0 mm error from around 5.5 seconds to 8 seconds. Once that drive current is removed from the motor windings at the 8 sec. mark, the rotor is relaxed and the brake cannot keep the rotor in its final driven position. This phenomenon causes a marginal increase steady-state error in varying magnitudes across the AMM range of travel, taking the steady-state error from ± 25 nm to upwards of ± 200 nm. This error is also always in the same direction due to the preload on the linear stage, and can be compensated in the control algorithm.

Summary of Achievements

The motor control electronics and accompanying firmware developed for this task greatly exceeded the expectations of the design team in meeting positioning accuracy and resolution requirements. Test results show that the Alignment Mirror Mechanism is essentially mechanically limited in its steady-state accuracy. Contributing factors to this include practical machining tolerances and assembly techniques. The resultant electronics and test results detailed in this paper will allow preceding tasks to build upon the realized shortcomings of the current AMM mechanical design and highlight possible sources of improvement.

7. LESSONS LEARNED

Mirror Configuration

Originally, light weighted mirrors were used. However, wavelength distortions caused the mirrors to be replaced with full size mirrors, which eliminated such distortions.

Ball Nut Stiffness

The ball nuts have less than one full turn of actively engaged balls interacting with the lead screw, primarily due to their small size. This was not obvious from the manufacturer's specifications; it was only detected when inspecting the hardware. The consequence is that the encoder's glass scale mounting arm, which is mounted at the ball nut, and extends downward parallel to the spindle, might not remain as rigidly parallel to the spindle as would have been if the ball nut was guided by multiple rows of balls. A minute swinging out of the encoder arm also has a displacement component in the axial direction, thus influencing the encoder reading as an unwanted side-effect.

Brake Induced Positional Shifts

With this disk brake, one active brake shoe pushes on the brake disk axially, while the opposing brake shoe is passive at a nominal distance below the brake disk. Even though the brake disk is waver thin (approximately .3mm), and deforms to touch the lower brake shoe when the brake is engaged, it is still possible to sense the axial position shift with the ultra sensitive position sensor. This positional shift also propagates through the spindle and influences the mirror's position. It can be factored out by software, but a new design should consider modifying the brake to avoid such positional shifts.

Redundant PZTs

The two PZTs were meant to be used independently, with each capable of actuating the brake. However, the flexures and the winding up of the material require a little more stroke than what a single PZT (12 μm stroke) can provide. Hence, both PZTs have to be energized to open the brake completely. This eliminated the redundancy of the system. In future models, 3 PZTs will be stacked on top of each other, so that two are available to actuate the brake, whereas the 3rd will be a redundant PZT.

Vibration Noise

During vibration testing, a pinging (chatter) noise was audible during vibration testing near peak amplitude values. Even though this noise turned out to be harmless, it originated from the brake shoes impacting the brake disk due to its close proximity; it caused that the vibration test was aborted, with investigation following to determine the source of this noise. This turned out to be quite an expensive distraction.

Refinement of PID Parameters

The resultant torque necessary to drive the Ballscrew turned out to be towards the low end of what the FPGA firmware was capable of driving without oscillation. The gains for the Proportional (P), Integral (I), and Derivative (D) parameters in the control software had been tailored to an application that contained a gearbox, thus requiring more torque. These

parameters simply act as a base, minimum value with external modification in the form of integer scalar values. This relatively low-torque system could occasionally find itself in an oscillatory state if the P term of the control loop was too high, and in practice, the P term of the control loop was always set to its minimum value. To remedy this problem and allow for performance margin and further optimization, the inherited PID firmware would have to be tailored to accommodate much lower torque applications.

8. SUMMARY

An opto-mechanical mirror positioning mechanism and its control electronics were developed, designed, fabricated, and tested. The devices enable accurate optical alignments of light beams for an interferometer. The mirror positioning and accuracy requirements were exceeded, the demonstrated positional accuracy is 0.7 arc-sec, which is quite remarkable for a device using a mechanical lead screw, and not a solid state device, such as PZT actuators.

REFERENCES

- [1] "SIM Lite Astrometric Observatory" JPL Publication 400-1360, 2/09.
- [2] Mitchell, Donald, K, "A Radiation-Hardened, High-Resolution Optical Encoder for Use in Aerospace Applications", IEEE Paper # 1561, IEEE Aerospace Conference, Big Sky, Mt, March 2008.

BIOGRAPHY



Dr. Bruno Jau is a Member of the Technical Staff at the Jet Propulsion Laboratory. He earned a Ph.D. in ME from the University of Southern California and a MS degree in ME from Michigan State University. His undergraduate work was done in Switzerland.

His areas of expertise are solid mechanics, mechanisms, CAD and manufacturing. He gained professional experiences in corporate, R&D, consulting and University environments, including a position as a Professor at Texas A&M University. Principal research activities include the development, design, and implementation of electromechanical systems and space instruments. He has published over 35 articles in these areas.

Dr. Jau joined JPL in 1985 and has worked in Robotics and Mechanical Engineering Sections since then. He was responsible for the mechanical development of several space flight instruments. He also developed, designed and implemented a variety of robotics prototypes, including an anthropomorphic telerobot system with a four fingered hand.



Colin McKinney received his B.S. degree in Electrical Engineering from Cal Poly, San Luis Obispo in 2008 and is currently pursuing his M.S.E.E. at the University of Southern California while employed full-time at the Jet Propulsion Laboratory. He is a member of the Advanced Instrument Electronics group under Mohammad Mojarradi at

JPL with a primary focus of analog and mixed-signal electronics design. He is also active in the research and development of the enabling technologies for low-noise extreme environment (wide-temperature, high radiation) instrumentation-quality circuit design and implementation.



Robert Smythe received his B.S. and M.S. in Electrical Engineering from the University of Washington. He has been employed by the Jet Propulsion Laboratory since 1999, involved predominantly in Motion Control, Dynamic Optical Systems, and device characterization for optical interferometry projects, such as the Keck Interferometer,

Terrestrial Planet finder, ST7, and the Space Interferometry Mission. His current role is the cognizant engineer in charge of Ground Support Electronics and Software for the Space Interferometry Mission.



Dean Palmer has been employed at the Jet Propulsion Laboratory since 1989 working primarily on control systems and interfaces for various optical interferometry projects, including the Palomar Testbed Interferometer, the Keck Interferometer, and the Space Interferometry Mission. In his current assignment, he has focused on FPGA designs for several key

system components. Dean studied Electrical Engineering at California Polytechnic State University, San Luis Obispo Interferometry Mission. In his current assignment, he has focused on FPGA designs for several key system components. Dean studied Electrical Engineering at California Polytechnic State University, San Luis Obispo.

ACKNOWLEDGEMENTS

The authors wish to thank their JPL colleagues and acknowledge their contributions in the development of the AMM mechanisms: Xin An, Testing - Zensheu Chang, Structure - Ben Doty, Dynamics - Dan Flores, Design - Renaud Goullioud, Management - John Guenther, Design - Steve Hankins, Electronics - Daniel Kahn, Mechanical -

John Koenig, Electronics - Gary Kuan, Optical - James Moore, Mechanical - John Shaw, Technician - Brian Trease, Mechanical

The research described in this paper was carried out at the Jet Propulsion Laboratory, California Institute of Technology, under a contract with the National Aeronautics and Space Administration.

Copyright 2010 California Institute of Technology

